Bulletin of Mathematical Biology (2007) 69: 1537–1565
DOI 10.1007/s11538-006-9175-8

ORIGINAL ARTICLE

Modeling Group Formation and Activity Patterns in Self-Organizing Collectives of Individuals

R. Eftimie[a,*], G. de Vries[a], M. A. Lewis[a,b], F. Lutscher[a,c]

[a] *Centre for Mathematical Biology, Department of Mathematical and Statistical Sciences, University of Alberta, Edmonton, Alberta T6G 2G1, Canada*
[b] *Centre for Mathematical Biology, Department of Biological Sciences, University of Alberta, Edmonton, Alberta T6G 2E9, Canada*
[c] *Department of Mathematics and Statistics, University of Ottawa, Ottawa ON, K1N 6N5, Canada*

Received: 13 March 2006 / Accepted: 20 September 2006 / Published online: 15 February 2007

Abstract We construct and analyze a nonlocal continuum model for group formation with application to self-organizing collectives of animals in homogeneous environments. The model consists of a hyperbolic system of conservation laws, describing individual movement as a correlated random walk. The turning rates depend on three types of social forces: attraction toward other organisms, repulsion from them, and a tendency to align with neighbors. Linear analysis is used to study the role of the social interaction forces and their ranges in group formation. We demonstrate that the model can generate a wide range of patterns, including stationary pulses, traveling pulses, traveling trains, and a new type of solution that we call zigzag pulses. Moreover, numerical simulations suggest that all three social forces are required to account for the complex patterns observed in biological systems. We then use the model to study the transitions between daily animal activities that can be described by these different patterns.

Keywords Nonlocal hyperbolic system · Group formation · Social interactions · Spatial patterns · Zigzag movement

1. Introduction

Communication between individuals, and, in particular, reception of information, is of crucial importance for group formation and group movement in self-organizing communities of animals. In this paper, we will derive a mathematical

*Corresponding author.
E-mail address: reftimie@math.ualberta.ca (R. Eftimie).

model for group formation and movement based on how animals receive information, and how this information influences the social interactions among them.

The study of animal aggregations (such as schools of fish, swarms of insects, etc.) has become a topic of great interest, especially in the past years (Gueron et al., 1996; Flierl et al., 1999; Okubo et al., 2001). Understanding aggregation has not only theoretical significance, but also more practical applications. For example, understanding schooling behavior can be useful in establishing fishing strategies (Radakov, 1973; Parrish, 1999), while understanding desert locust aggregations can be useful in managing and controlling this species' outbreaks (Uvarov, 1966; Simpson et al., 1999). More recently, aggregative, schooling and swarming behavior has attracted the attention of physicists, computer scientists, and engineers interested in autonomous robots and traffic flow in intelligent transportation systems (Kube and Zhang, 1993; Kerner and Konhäuser, 1994; Vicsek et al., 1999; Gazi and Passino, 2002).

There are two kinds of factors that influence group formation: external factors that, for example, give rise to chemotaxis, phototaxis, or thermotaxis, and internal factors, which are social forces that act among individuals (Breder, 1954; Warburton and Lazarus, 1991; Huth and Wissel, 1994; Beecham and Farnsworth, 1999; Simpson et al., 1999). The present research focuses on the internal factors that lead to group formation. We consider the following factors: attraction toward other individuals, repulsion from others, and the tendency to align with neighbors (i.e., to adjust the movement direction to that of neighbors). Each of these forces act over a certain spatial scale or within a certain range of influence.

Over the past 50 years, a large number of mathematical models have been derived for the purpose of better understanding animal aggregations (Breder, 1954; Okubo, 1986; Pfistner, 1990; Huth and Wissel, 1994; Gueron et al., 1996; Edelstein-Keshet et al., 1998; Mogilner and Edelstein-Keshet, 1999; Couzin et al., 2002; Lutscher, 2002; Mogilner et al., 2003; Topaz et al., 2006, and references therein). These models fall into two frameworks: Lagrangian models (individual-based models) and Eulerian models (continuum models).

In the Lagrangian approach, a set of decision rules that govern the movements of individuals is given (Reynolds, 1987; Huth and Wissel, 1994; Reuter and Breckling, 1994; Gueron et al., 1996; Vabø and Nøttestad, 1997; Couzin et al., 2002). Most of these models are in two spatial dimensions, and include all three types of social interactions that alter the position of an individual: attraction, repulsion, and alignment (Reynolds, 1987; Huth and Wissel, 1994; Reuter and Breckling, 1994; Couzin et al., 2002). Many Lagrangian models focus on the structure of the group (e.g., geometry of the group, degree of polarization, etc.), and simulations show very close agreement between these structures and those observed in nature (Reynolds, 1987; Huth and Wissel, 1994; Vabø and Nøttestad, 1997; Couzin et al., 2002). Couzin et al. (2002), for example, described four types of groups: swarm, torus, dynamic parallel groups, and highly parallel groups, and then looked at the transition between these types of group structure, as the size of the interaction zones is varied. Due to analytical difficulties in studying Lagrangian models, as well as some computational limitations, this approach is applied mostly to small groups of organisms.

On the other hand, Eulerian models are used to study the dynamics of the density of individuals, which is typically described by partial differential equations. Usually, these models are applied to large populations of insects, fish, bacteria, and so forth. Continuum models for animal aggregations can be divided into two categories: parabolic and hyperbolic equations. For both types of models, the social interactions between group members can be local, when immediate neighbors or local effects of the environment are important (Edelstein-Keshet et al., 1998; Lutscher, 2002; Lutscher and Stevens, 2002), or nonlocal, when distant individuals or nonlocal effects of the environment play an important role (Mogilner and Edelstein-Keshet, 1996, 1999; Bressloff, 2004; Topaz and Bertozzi, 2004; Topaz et al., 2006).

Parabolic models, which comprise the majority of continuum models, usually incorporate nonlocal attractive and repulsive terms (Mogilner and Edelstein-Keshet, 1999; Topaz and Bertozzi, 2004; Topaz et al., 2006). These models include two components of movement: a random one, modeled by diffusion, and a nonrandom component, modeled by advection (Okubo et al., 2001; Topaz et al., 2006). To date, the models have been usually used to investigate one behavior at a time, such as traveling band solutions (Mogilner and Edelstein-Keshet, 1999), stationary solutions (Topaz et al., 2006), or vortex-like groups (Topaz and Bertozzi, 2004).

There are a few parabolic models that also incorporate alignment, two such examples being proposed by Mogilner and Edelstein-Keshet (1996) and Bressloff (2004). Both models show three types of spatial patterns: alignment without aggregation, aggregation without alignment, and patches of aligned objects.

A few hyperbolic models analyze the effect of alignment on group formation and movement, using local (Lutscher, 2002) or nonlocal (Pfistner, 1990, 1995) terms. Studying the swarming behavior of Myxobacteria, Pfistner (1990) derived a system of first-order hyperbolic equations that considered nonlocal density-dependent turning rates, and used it to investigate the formation of stationary swarms. Later, Pfistner (1995) modified the model by introducing free boundary conditions for the swarm edges, and studied swarm cohesion numerically, analyzing expansion and retraction of boundaries. The new element introduced by these two models is a straightforward way to incorporate alignment into the turning rates. Starting with the same modeling procedure as Pfistner, we propose to incorporate other social forces that affect these rates: repulsion and attraction.

To incorporate these social interactions, we focus on communication. Animal communication uses different signals: visual, acoustic, chemical, or tactile signals (Marler, 1967; Partan and Marler, 2005). Both emission and reception of signals can be unidirectional or omnidirectional, depending on the signal. In the formulation of our model, we will be concerned only with the reception of these signals, since it represents the basis for animal communication (Marler, 1967; Partan and Marler, 2005). Moreover, some signals are efficient on short ranges (e.g., repulsion range), while others are efficient on long ranges (e.g., attraction range). We use the directionality of the signals, as well as the ranges on which signals have effect, to define the social interactions. In this paper, we will consider only a specific case of animal communication, by assuming that both attraction and repulsion involve omnidirectional signals, while alignment involves only unidirectional signals.

The aim of this paper is thus to include all three social interactions into a continuum model for animal movement, and investigate the resulting spatial patterns and the possible transitions between them. To this end, we formulate a hyperbolic model similar to the one by Pfistner (1990), where the turning rates depend on all three social forces, namely attraction, repulsion, and alignment, in a way that reflects the characteristics of the communication process. We formulate simple rules by which the perceived signals are translated into movement behavior. We use linear analysis and numerical simulations to investigate the different possible types of group structures that arise. We show that only the interactions between all three forces can account for the complex patterns observed in biological systems. When all three social interactions are present, the model displays four types of solutions: stationary pulses, traveling pulses, traveling trains, and a new type of solution that we call zigzag pulses.

The paper is organized as follows. Section 2 contains the model derivation. Section 3 focuses on the spatially homogeneous steady states and their local stability. We also use the dispersion relation to gain insights into the effect of different interaction ranges on group formation. In Section 4, via numerical simulations, we study the spatially nonhomogeneous solutions displayed by our system. We also discuss the transition between different daily activities described by the numerical solutions. In Section 5, we compare the results with actual activity patterns observed in nature. We conclude with a general discussion in Section 6.

2. Model description

We start with the hypothesis made by many Lagrangian models, namely that each individual interacts with its neighbors via three social forces, attraction, repulsion, and alignment. We further assume that each of these forces has a different interaction range (Fig. 1(a)). More specifically, we assume that an individual changes direction to approach other individuals if they are within its attraction range, or to avoid collision if they are within its repulsion range (Fig. 1(a)). Moreover, an individual turns to match its orientation to its neighbors' direction of movement (i.e., to align) if they are within its alignment range.

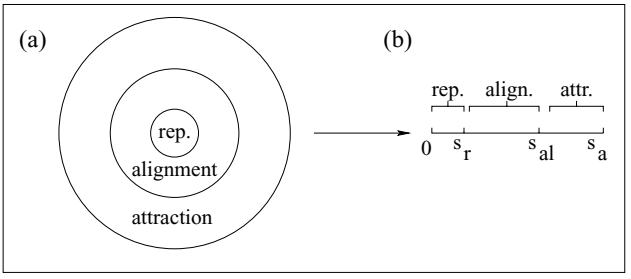

Fig. 1 Illustration of the repulsion (s_r), alignment (s_{al}), and attraction (s_a) zones: (a) two-dimensional case; (b) one-dimensional case. It is biologically realistic to have $s_r < s_{al} < s_a$.

Since we derive a one-dimensional model, the concentric circles that usually describe the interaction ranges in two-dimensional Lagrangian models (Fig. 1(a)) are replaced by intervals on the real number line (Fig. 1(b)).

Using the correlated random walk approach (Kac, 1974; Segel, 1977; Othmer et al., 1988; Pfistner, 1990), we derive the following hyperbolic system of conservation laws that describe the evolution of densities of left-moving and right-moving individuals:

$$\begin{aligned}
\partial_t u^+(x,t) + \partial_x(\gamma u^+(x,t)) &= -\lambda^+ u^+(x,t) + \lambda^- u^-(x,t),\\
\partial_t u^-(x,t) - \partial_x(\gamma u^-(x,t)) &= \lambda^+ u^+(x,t) - \lambda^- u^-(x,t),\\
u^\pm(x,0) &= u_0^\pm(x), x \in \mathbf{R}.
\end{aligned} \tag{1}$$

Here $u^+(x,t)$ ($u^-(x,t)$) is the density of individuals at (x,t) that move to the right (left), and γ is their constant speed. We have denoted by λ^+ (λ^-) the turning rates for the individuals that were initially moving to the right (left) and then turn to the left (right).

While the model, represented by Eq. (1), is formally identical with the model by Pfistner (1990), the biological processes considered in the turning functions differ considerably. Pfistner only modeled alignment and used turning functions that were positive, unbounded, and increasing functions of the signals perceived from neighbors within a certain perception distance.

We, however, assume that all three social interactions influence the turning rates, so that $\lambda^\pm$ models attraction, repulsion, and alignment as a response of an individual to the signals perceived from its neighbors. We assume that stronger interaction forces lead to higher turning rates (to avoid collision, for example, in case of high repulsion), and we consider the turning rates to be bounded monotone functions of the perceived signals $y^\pm$, which are emitted by individuals moving to the right (u^+) and to the left (u^-) :

$$\begin{aligned}
\lambda^\pm(y^\pm) &= \lambda_1 + \lambda_2 f(y^\pm[u^+,u^-])\\
&= (\lambda_1 + \lambda_2 f(0)) + \lambda_2(f(y^\pm[u^+,u^-]) - f(0)),
\end{aligned} \tag{2}$$

where $\lambda_1 + \lambda_2 f(0)$ is a baseline random turning rate, and $\lambda_2(f(y^\pm) - f(0))$ is a bias turning rate. We choose f to be a dimensionless, bounded, and increasing function of the dimensionless functionals $y^\pm[u^+,u^-]$ that incorporate nonlocal interaction terms:

$$y^\pm[u^+,u^-] = y_r^\pm[u^+,u^-] - y_a^\pm[u^+,u^-] + y_{al}^\pm[u^+,u^-]. \tag{3}$$

Here, $y_{\mathrm{r}}^\pm$, $y_{\mathrm{al}}^\pm$, and $y_{\mathrm{a}}^\pm$ denote the repulsion, alignment, and attraction terms that influence the likelihood of turning to the left (+) or to the right (−). We will specify the dependence of these terms on u^+ and u^- shortly. The three interactions are introduced in an additive manner, with repulsive and attractive terms having opposite effects. Throughout this paper, we use the following turning function (Fig. 2):

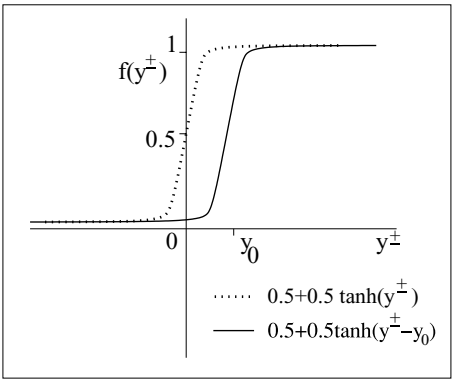

Fig. 2 A turning function that satisfies our assumptions: increasing, positive, and bounded. The constant y_0 shifts the graph to the right such that for $y^{\pm} = 0$, there is only a small random turning.

$$f(y^{\pm}[u^+, u^-]) = 0.5 + 0.5 \tanh(y^{\pm}[u^+, u^-] - y_0), \tag{4}$$

where the constant y_0 is chosen such that $f(0) \ll 1$ and the random turning dominates the movement. In this case, the baseline turning can be approximated by λ_1, and the change in turning rate due to interactions by $\lambda_2 f(y^{\pm})$.

In order to describe the dependence of the social interactions, $y_{\mathrm{r}}^{\pm}$, $y_{\mathrm{al}}^{\pm}$, and $y_{\mathrm{a}}^{\pm}$, on u^+ and u^-, we look at the way organisms perceive and integrate information. As mentioned in Section 1, we assume that both direction and spatial range of signals define the social interactions. We introduce four parameters that measure the information received from the right or left: $p_{\mathrm{r}}^{\pm}$ and $p_{\mathrm{l}}^{\pm}$. The superscript $(\pm)$ refers to direction in which the sender of the information moves, and the subscript (r, l) refers to the direction from which the signal is received (right, left) (Fig. 3). Later, for the sake of simplicity, the analysis will concentrate on special cases. By way of example, suppose that the individual positioned at (x, t) moves to the right $(+)$ (Fig. 3(a)), and that it receives information from other individuals located to its right, at $x + s$, and located to its left, at $x - s$. Also, suppose that this individual perceives a stronger signal from the right than from the left, that is, $(p_{\mathrm{r}}^{+}u^{+} + p_{\mathrm{r}}^{-}u^{-})(x + s) > (p_{\mathrm{l}}^{-}u^{-} + p_{\mathrm{l}}^{+}u^{+})(x - s)$. If the signal comes from within the repulsion zone, then it will turn to avoid those neighbors that are to its right, regardless of their orientation. If the signal comes from within the attraction zone, it will continue moving in the same direction.

For simplicity, we choose $p_{\mathrm{r}}^{+} = p_{\mathrm{r}}^{-} = p_{\mathrm{r}}$ and $p_{\mathrm{l}}^{+} = p_{\mathrm{l}}^{-} = p_{\mathrm{l}}$. If we sum the information from all neighbors ($s \in (0, \infty)$), we can translate the diagrams from Fig. 3 into the following nonlocal terms that describe the social interactions:

$$y_{\mathrm{r,a}}^{+}[u^+, u^-] = q_{\mathrm{r,a}} \int_0^{\infty} K_{\mathrm{r,a}}(s) \left(p_{\mathrm{r}} u(x + s) - p_{\mathrm{l}} u(x - s)\right) \mathrm{d}s, \tag{5}$$

$$y_{\mathrm{r,a}}^{-}[u^+, u^-] = q_{\mathrm{r,a}} \int_0^{\infty} K_{\mathrm{r,a}}(s) \left(p_{\mathrm{l}} u(x - s) - p_{\mathrm{r}} u(x + s)\right) \mathrm{d}s, \tag{6}$$

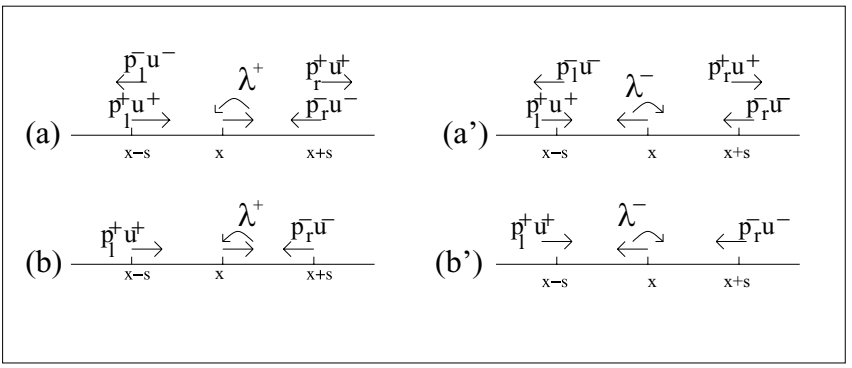

Fig. 3 Description of possible turning functions. Cases (a)–(b) depict a switch in movement direction from right to left, while cases (a′)–(b′) depict the switch in movement direction from left to right. Cases (a), (a′) describe attraction and repulsion, while (b) and (b′) describe alignment. Here u^+ (u^-) represents the density of individuals moving right (left), and λ^+ (λ^-) is the probability of turning to the left (right), when initially the individual at x was moving to the right (left). The other parameters, $p_l^{\pm}$ and $p_r^{\pm}$, represent signals received from the left (subscript l) and the right (subscript r), from other neighbors that are moving to the left (superscript "−") or to the right (superscript "+").

$$y_{al}^{+}[u^+, u^-] = q_{al} \int_0^{\infty} K_{al}(s)(p_r u^-(x+s) - p_l u^+(x-s))\mathrm{d}s, \tag{7}$$

$$y_{al}^{-}[u^+, u^-] = q_{al} \int_0^{\infty} K_{al}(s)(p_l u^+(x-s) - p_r u^-(x+s))\mathrm{d}s, \tag{8}$$

where $K_i(s), i \in \{\mathrm{a}, \mathrm{r}, \mathrm{al}\}$ are interaction kernels, with support inside the interval $[0, \infty)$, that describe how signals from different distances are weighed. The parameters q_a, q_r, and q_{al} represent the magnitudes of the attraction, repulsion, and alignment forces, respectively. For attraction and repulsion, the total density of organisms at a specific position in space is important: $u(x \pm s, t) = u^+(x \pm s, t) + u^-(x \pm s, t)$, $s > 0$. We assume here that as long as the individual located at x moves toward neighbors that are in the repulsion zone, it will turn to avoid collision, no matter what the movement direction of those neighbors is. Similarly, the individual is attracted by neighbors within its attraction zone, regardless of their orientation. For alignment, however, we assume that an individual responds *only to neighbors moving toward it.* For example, for y_{al}^{+} (Eq. (7)), we assume that a right-moving individual at point x will turn around only if $p_r u^-(x+s)$ is large relative to $p_l u^+(x-s)$.

In summary, the right-hand sides of Eqs. (5)–(8) describe how the individual at (x, t) weighs information received from its right and left neighbors. The only difference between the repulsion term ($y_r^{\pm}[u^+, u^-]$) and the attraction term ($y_a^{\pm}[u^+, u^-]$) is in the range over which the two kernels $K_r(s)$ and $K_a(s)$ have influence (Fig. 4). Recall that since repulsion and attraction have opposite effects, these two terms enter the turning function (Eq. (3)) with different signs.

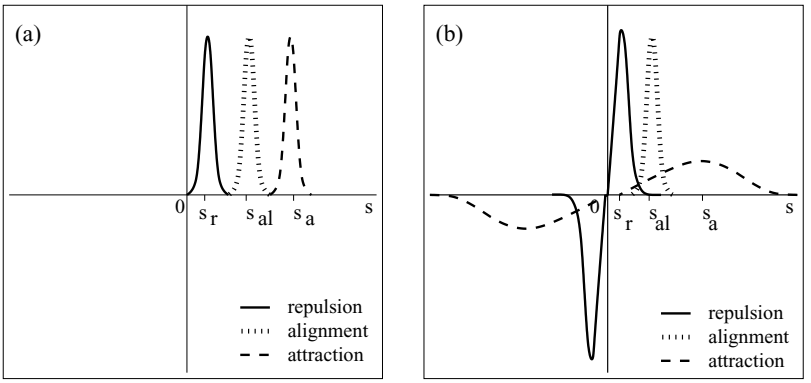

Fig. 4 Examples of kernels used for numerical simulations. These kernels describe how signals from different distances are weighed. (a) translated Gaussian kernels for attraction, repulsion and alignment, described by equations (9); (b) odd kernels for attraction and repulsion, and a translated Gaussian kernel for alignment (Eqs. (11) and (9)). Both types of kernels are defined on $(-\infty, \infty)$. The interaction ranges on which these kernels have an effect, satisfy $s_r < s_{al} < s_a$. The s_r, s_{al}, and s_a represent half the length of the interaction ranges depicted in Fig. 1.

A possible choice for the interaction kernels is translated Gaussian kernels (Fig. 4(a)):

$$K_i(s) = \frac{1}{\sqrt{2\pi m_i^2}} \exp(-(s - s_i)^2 / (2m_i^2)), \quad i = \text{r, a, al}, \quad s \in [0, \infty), \tag{9}$$

where s_r, s_{al}, and s_a represent half the length of the interaction ranges, for the repulsion, alignment, and attraction terms, respectively. The constants m_i are chosen such that the support of more than 98% of the mass of the kernels is inside the interval $[0, \infty)$: $m_i = s_i/8$, $i \in \{\text{r, al, a}\}$. In this case, the integrals defined on $[0, \infty)$ can be approximated by integrals on $(-\infty, \infty)$.

To simplify the model equations for the purpose of analysis, we choose $p_l = p_r$ (the case $p_l \neq p_r$ will be dealt with in Section 4). Moreover, these parameters will be incorporated into the magnitudes of repulsion q_r, alignment q_{al}, and attraction q_a. Then, if we extend K_r and K_a to odd kernels on the whole real line, Eqs. (5) and (6) can be rewritten as

$$y^{\pm}_{r,a}[u^+, u^-] = q_{r,a} \int_{-\infty}^{\infty} K_{r,a}(s) u(x \pm s)\, ds. \tag{10}$$

A second possible choice, similar to Mogilner and Edelstein-Keshet (1999), is to define the attraction and repulsion kernels by (Fig. 4(b))

$$K_i(s) = \frac{s}{2s_i^2} \exp(-s^2 / (2s_i^2)), \quad i = \text{a, r}, \quad s \in (-\infty, \infty). \tag{11}$$

The two model formulations (kernels on the half-line, and odd extensions on the full-line) are equivalent. Equation (10) together with Fig. 4(b) show that if a

right- or left-moving individual perceives many neighbors ahead of it, the likelihood of turning will increase in case of repulsion, or decrease in case of attraction. Conversely, the perception of many neighbors behind that individual will lead to a decrease in the turning rates in case of repulsion, or to an increase in these rates in case of attraction. Since an individual needs to distinguish movement directions and not just densities of its neighbors (i.e., u^+, u^- vs. u) in order to align, we do not use odd alignment kernels.

Altogether, Eqs. (3)–(11) describe aspects of how an organism at (x, t) makes the decision to turn: it turns to avoid collision if the majority of the stimuli received originate within the repulsion zone, or to approach other individuals if the majority of the stimuli received originate within the attraction zone. If the majority of the stimuli originate within the alignment zone, the individual will turn to align itself according to the prevailing movement direction of the neighbors moving toward it. For a summary of the full model please see Appendix B.

The full model has 14 parameters. For the convenience of the reader, we list these parameters in Table 1. While nondimensionalizing allows us to reduce the number of parameters to 10, the analysis is no more difficult when dealing with the dimensional form, which we will do in the following. Moreover, the original parameters are biologically motivated. It is easier to interpret the results of the model (Sections 3.3 to 6) by talking about the model using these parameters in their original biological context.

3. Spatially homogeneous steady states and their local stability

A standard approach in the study of animal self-organization is to assess the possibility of pattern formation. To do so, one determines conditions under

Table 1 A list with the model parameters used during the simulations

Parameter	Description	Units	Fixed value
γ	Speed	L/T	No: $\gamma \in (0.015, 0.1)$
λ_1	Turning rate. It approximates the baseline turning rate: $\lambda_1 + \lambda_2 f(0)$	$1/T$	No: $\lambda_1 \in (0.2, 1.33)$
λ_2	Turning rate. It approximates the bias turning rate: $\lambda_2 \left(f(y^{\pm}) - f(0)\right)$	$1/T$	No: $\lambda_2 \in (0.9, 6)$
y_0	Shift of the turning function	1 (nondim.)	Yes: $y_0 = 2$
q_a	Magnitude of attraction	L/N	No: $q_a \in (0, 15)$
q_{al}	Magnitude of alignment	L/N	No: $q_{al} \in (0, 2)$
q_r	Magnitude of repulsion	L/N	No: $q_r \in (0, 2)$
s_a	Attraction range	L	Yes: $s_a = 1$
s_{al}	Alignment range	L	Yes: $s_{al} = 0.5$
s_r	Repulsion range	L	Yes: $s_r = 0.25$
m_a	Width of attraction kernel	L	Yes: $m_a = 1/8$
m_{al}	Width of alignment kernel	L	Yes: $m_{al} = 0.5/8$
m_r	Width of repulsion kernel	L	Yes: $m_r = 0.25/8$
A	Total population size	N	yes: $A = 2$

Note. The two parameters for the strength of information received from left/right, namely p_l/p_r are already incorporated into the magnitudes of attraction q_a, alignment q_{al}, and repulsion q_r. T represents the unit time, L is the unit space, and N is the number of individuals.

which the spatially uniform steady state loses its stability via growth of small spatial perturbations. The loss of stability through real or complex eigenvalues suggests a means by which aggregation or, respectively, dispersive waves, can occur.

We start by determining the spatially homogeneous steady states in Section 3.1. In Section 3.2, we derive the dispersion relation corresponding to these steady states, and use it first to study the stability of these solutions and later, in Section 3.3, to study the effect of the length of interaction ranges on the stability.

3.1. Steady states

We look for the spatially homogeneous steady states $u^+(x,t) = u^*$ and $u^-(x,t) = u^{**}$, with total density $A = u^* + u^{**}$, and obtain the steady state equation for system represented by Eq. (1),

$$h(u^*; q_{\rm al}, \lambda, A) = 0, \tag{12}$$

where h is being defined as

$$\begin{aligned} h(u^*; q_{\rm al}, \lambda, A) := & -u^* \left(1 + \lambda \tanh(Aq_{\rm al} - 2u^* q_{\rm al} - y_0)\right) \\ & + (A - u^*)\left(1 + \lambda \tanh(-Aq_{\rm al} + 2u^* q_{\rm al} - y_0)\right), \end{aligned} \tag{13}$$

and

$$\lambda = \frac{0.5\lambda_2}{0.5\lambda_2 + \lambda_1}. \tag{14}$$

Although the model involves a large number of parameters, only four of them arise in this steady state equation: A, λ, $q_{\rm al}$, and y_0. Only the first three parameters will be varied, y_0 being fixed by our choice for the turning function. We look at the effect of varying A since we expect that the higher the population density, the stronger the interindividual interactions. Therefore, we expect A to influence the aggregation process. A similar explanation holds for $q_{\rm al}$. Intuitively, the turning rates also influence the formation of population clusters. The effects of varying all these parameters are presented in Fig. 5, through three bifurcation diagrams.

Since we have chosen $K_{\rm r,a}$ to be odd kernels,

$$\int_{-\infty}^{\infty} K_{\rm r,a}(s)(u^* + u^{**})\,{\rm d}s = 0. \tag{15}$$

Hence, the attraction and repulsion terms vanish, and the only social interaction that determines the number of possible steady states is alignment. When $q_{\rm al} = 0$, the only steady state is $(u^+, u^-) = (A/2, A/2)$. For $q_{\rm al} \neq 0$, Eq. (12) can have one,

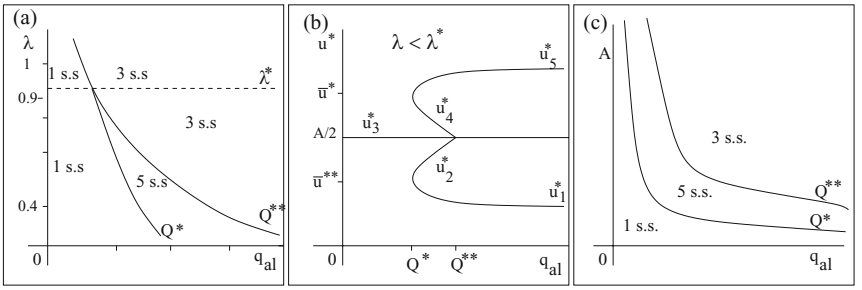

Fig. 5 Bifurcation diagrams for the steady state equation. (a) Two-parameter bifurcation diagram in $(q_{\rm al}, \lambda)$ space: the threshold values λ^*, Q^* and Q^{**} determine the number of possible steady states; $A = 2$ and $y_0 = 2$ are fixed parameters. (b) Bifurcation diagram in the five steady state regime (i.e., $\lambda < \lambda^*$): $\bar{u}^*$ and $\bar{u}^{**} = A - \bar{u}^*$ are the two critical states that appear at Q^* as we increase $q_{\rm al}$. These two states can take up to five values each: $\bar{u}^* \in \{u_1^*, u_2^*, u_3^*, u_4^*, u_5^*\}$, and $\bar{u}^{**} = A - \bar{u}^*$. Here $A = 2$, and λ is given by Eq. (14), with $\lambda_1 = 0.2$ and $\lambda_2 = 0.9$. (c) Two-parameter bifurcation diagram in $(q_{\rm al}, A)$ space: $q_{\rm al}$ and A have similar effects on the number of spatially homogeneous solutions; Here $\lambda_1 = 0.2$, $\lambda_2 = 0.9$.

three, or five solutions (Fig. 5), depending on the values of λ. More precisely, there is a threshold value

$$\lambda^* = \frac{-1 + 3\tanh(y_0)^2}{2\tanh(y_0)} \tag{16}$$

such that for $\lambda > \lambda^*$ (i.e., for λ_1 much smaller than λ_2), there are up to three solutions, while for $\lambda < \lambda^*$, there are up to five solutions (Fig. 5(a)). We will denote these five solutions by u_i^*, $i = 1..5$. Therefore, the spatially homogeneous steady states generically denoted by $(u^*, u^{**}) = (u^*, A - u^*)$ can be any of the following pairs: (u_1^*, u_5^*), (u_5^*, u_1^*), (u_2^*, u_4^*), (u_4^*, u_2^*), or (u_3^*, u_3^*).

In the remainder of this paper, we fix the ratio λ_1/λ_2 with $\lambda_1 << \lambda_2$, so that $\lambda < \lambda^*$, which implies that there can be up to five steady states (Fig. 5(a) and (b)). The other two threshold values for $q_{\rm al}$ from Fig. 5, namely Q^* and Q^{**}, are as follows: Q^{**} is given explicitly by

$$Q^{**} = \frac{-1 + \lambda\tanh(y_0)}{\lambda A(-1 + \tanh(y_0)^2)}, \tag{17}$$

while Q^* is a decreasing function of λ, defined implicitly by

$$\frac{\partial^3 h(A/2; Q^*, \lambda, A)}{\partial q_{\rm al}^3} = 0. \tag{18}$$

The dependence of u^* on $q_{\rm al}$ is shown in Fig. 5(b), in the five steady states regime. As alignment becomes very large, and, in particular, $q_{\rm al} \to \infty$, the three homogeneous steady states are $u^{\pm} \in \{A(1-\lambda)/2, A/2, A(1+\lambda)/2\}$. Figure 5(c) illustrates the dependence of the number of steady states on both A and $q_{\rm al}$, again in the five steady states regime. This last figure suggests that $q_{\rm al}$ and A have similar effects on

the number of steady states: for small q_{al} or A, it is possible to have only one steady state $(u^*, u^{**}) = (A/2, A/2)$, while for large q_{al} or large A, there are three steady states.

3.2. *Local stability*

Once we know the possible homogeneous steady states, the next step is to study the local stability of these solutions under small perturbations caused by spatially non-homogeneous terms: $u^+(x,t) = u^* + u_p(x,t)$ and $u^-(x,t) = u^{**} + u_m(x,t)$, with $(u^*, u^{**} = A - u^*)$ being the generic notation for the spatially homogeneous steady states. We approach the problem of pattern formation by choosing to define Eq. (1) on a bounded domain of length L with wrap-around boundary conditions for the nonlocal influence terms. This yields a problem with a discrete spectrum, and also approximates the process of pattern formation on an unbounded domain when L is large. In this case, the interaction kernels are, as in Robbins (2003),

$$\Gamma_j(s) = \sum_{n=-\infty}^{+\infty} K_j(s + nL), \quad j \in \{\mathrm{r}, \mathrm{al}, \mathrm{a}\}. \tag{19}$$

The Fourier transform of the kernel $K_j(s)$ is given by

$$\hat{K_j}^{\pm}(k) = \int_{-\infty}^{\infty} K_j(s) \mathrm{e}^{\pm \mathrm{i}ks}\, \mathrm{d}s. \tag{20}$$

Also, we define

$$\hat{\Gamma_j}^{\pm}(k) := \int_{-L/2}^{L/2} \Gamma_j(s) \mathrm{e}^{\pm \mathrm{i}ks} \mathrm{d}s. \tag{21}$$

For large L, and in particular for $L \to \infty$, $\hat{\Gamma_j}^{\pm}(k)$ can be approximated by $\hat{K_j}^{\pm}(k)$ (see Appendix A):

$$\lim_{L\to\infty} \int_{-L/2}^{L/2} \Gamma_j(s) \mathrm{e}^{\pm \mathrm{i}ks}\, \mathrm{d}s = \hat{K_j}^{\pm}(k) \tag{22}$$

Due to this correspondence, we will work on a large finite domain $[0, L]$, and use $\hat{K_j}(k)$ to approximate interactions on finite domain by interactions on infinite domain. For the remainder of the paper, we will use the interaction kernels defined by Eq. (9) (for alignment) and Eq. (11) (for attraction and repulsion). The kernels are chosen such that the support of more than 98% of the kernels is small with respect to the length of the domain. The periodic boundary conditions that complete the description of the model on a finite domain are given by

$$u^+(0,t) = u^+(L,t), \; u^-(0,t) = u^-(L,t). \tag{23}$$

We let $u_{p,m}(x,t) \propto e^{\alpha t + ikx}$, with the discrete wavenumber $k = 2n\pi/L, n \in \mathbf{N}$, and the growth rate α, and substitute these expressions into the system, represented by Eq. (1), to obtain the dispersion relation:

$$2\alpha_{1,2}(k) = C(k) \pm \sqrt{C(k)^2 - D(k)}, \tag{24}$$

where

$$\begin{aligned}
C(k) &= -2(\lambda_1 + \lambda_2 0.5) - \lambda_2 \left(f(M_1) + f(-M_1) \right) \\
&\quad + \lambda_2 q_{\mathrm{al}} B(\hat{K}_{\mathrm{al}}^{+}(k) + \hat{K}_{\mathrm{al}}^{-}(k)), \\
D(k) &= 4\gamma^2 k^2 - 4\gamma i k h_2 - 8\gamma k \lambda_2 B(q_{\mathrm{r}} \hat{K}_{\mathrm{r}}^{+}(k) - q_{\mathrm{a}} \hat{K}_{\mathrm{a}}^{+}(k)) \\
&\quad + 8\gamma i k \lambda_2 B q_{\mathrm{al}} (\hat{K}_{\mathrm{al}}^{-}(k) - \hat{K}_{\mathrm{al}}^{+}(k)), \\
B &= u^* f'(M_1) + u^{**} f'(-M_1), \\
M_1 &= q_{\mathrm{al}}(u^{**} - u^*), \\
f(u) &= 0.5 \tanh(u - y_0), \\
f'(u) &= 0.5 - 2 f^2(u), \\
h_2 &= \lambda_2 \left(f(-M_1) - f(M_1) \right).
\end{aligned}$$

Here, $\hat{K}_j$, $j \in \{\mathrm{a}, \mathrm{r}, \mathrm{al}\}$ are the Fourier transforms of the interaction kernels, represented by Eq. (11) (for attraction and repulsion), and Eq. (9) (for alignment):

$$\hat{K_j}^{+}(k) = \int_{-\infty}^{\infty} K_j(s) e^{iks_j} \, \mathrm{d}s = iks_j \exp\left(-k^2 s_j^2/2 \right), \quad j = \mathrm{a}, \mathrm{r}, \tag{25}$$

$$\hat{K_{\mathrm{al}}}^{\pm}(k) = \int_{-\infty}^{\infty} K_{\mathrm{al}}(s) e^{\pm i k s_{\mathrm{al}}} \, \mathrm{d}s = \exp(\pm i s_{\mathrm{al}} k - k^2 m_{\mathrm{al}}^2/2). \tag{26}$$

Equation (24) shows that the steady state (u^*, u^{**}) is locally unstable, i.e., $\mathrm{Re}(\alpha_1(k)) > 0$, when $C(k) > 0$ or $D(k) < 0$. The first term, $C(k)$, is positive when λ_2 is large. For $D(k)$ to be negative, it requires either a large λ_2, or attraction to be larger than repulsion: $q_{\mathrm{a}} \hat{K}_{\mathrm{a}}(k) > q_{\mathrm{r}} \hat{K}_{\mathrm{r}}(k)$. If we focus now on each of the five solutions of Eq. (12) u_i^*, $i = 1..5$, we notice that Eq. (24) is important for the stability of $u_{1,5}^*$ for $q_{\mathrm{al}} > Q^*$, and of u_3^* for $q_{\mathrm{al}} < Q^{**}$. However, the stability of $u_{2,4}^*$ as well as u_3^* when $q_{\mathrm{al}} > Q^{**}$ is given not only by Eq. (24), but also by the domain length L. When the domain length becomes very large, and, in particular, $L \to \infty$, the first wavenumber $k_1 = 2\pi/L$ approaches zero. Consequently $C(k_1)$ approaches

$$C(0) = -2(\lambda_1 + \lambda_2 0.5) + \lambda 2(f(M_1) + f(-M1)) + 2\lambda_2 q_{\mathrm{al}} B. \tag{27}$$

In this case, u_2^* and u_4^*, as well as u_3^* for $q_{al} > Q^{**}$, are always unstable. More precisely, for $u^* = u_3^*$, the condition $q_{\mathrm{al}} > Q^{**}$ is equivalent to $C(0) > 0$, which means

that u_3^* is locally unstable. The steady state $u^* = u_2^*$ (or $u^* = u_4^*$) and $u^{**} = A - u^*$, is given implicitly as a solution of the system

$$h(\bar{u}^*; Q^*, \lambda, A) = 0, \quad \frac{\partial h(\bar{u}^*; Q^*, \lambda, A)}{\partial q_{\rm al}} = 0. \tag{28}$$

By studying the graph of $h(u)$, it can be deduced that the condition $q_{\rm al} \in (Q^*, Q^{**})$ requires that $\frac{\partial h(u;q_{\rm al},\lambda,A)}{\partial q_{\rm al}} > 0$, for any $u \in (\bar{u}^*, A/2)$. But this inequality is nothing else than $C(0) > 0$, which again, leads to instability. Therefore, for large L, $u_{2,3,4}^*$ are locally unstable, even in the absence of attraction, or for small turning rates. This ensures that we have a standard subcritical pitchfork bifurcation, as shown in Figs. 5(b) and 7.

Figure 6(a)–(f) shows examples of the dispersion relation for the system, represented by Eq. (1). The solid curve represents $\mathrm{Re}(\alpha_1)$, while the dashed curve represents $\mathrm{Im}(\alpha_1)$. We observe that for cases (a), (c), and (e), $\mathrm{Im}(\alpha_1(k)) \neq 0$, while for (b), (d), and (f), $\mathrm{Im}(\alpha_1(k)) = 0$ for some $k > 0$. Note that for the total density to be preserved, we require $k \neq 0$. Therefore, cases (e) and (f) do not contradict the conservation of the total density. The emergence of the first wavenumber k_1 (i.e., $\mathrm{Re}(\alpha(k_1)) > 0$) (see Fig. 6(a) and (b)) is the result of large attraction, while the emergence of k_i, $i \gg 1$ (Fig. 6(c) and (d)) is the result of large turning rates. Therefore, when attraction is large, we would expect the emergence of one group. When the turning rates λ_1 and λ_2 are large, we would expect the emergence of i small groups, where $i \gg 1$. The last two cases (Fig. 6(e) and (f)) show the dispersion relation corresponding to $u_{2,4}^*$ for $q_{\rm al} \in (Q^*, Q^{**})$, and to u_3^* for $q_{\rm al} > Q^*$, when the domain length L is large. As we can see here, the first wavenumber k_1 is always unstable, provided that the domain length is large enough. In this case, k_1 is very close to 0, and we have already seen that $C(0) > 0$, which implies instability.

The results concerning the steady states and the effect of the attraction, alignment, and total population size on their stability are summarized in Fig. 7. The solid curve represents stable steady states, while the dashed curve represents unstable steady states (i.e., $\mathrm{Re}(\alpha(k)) \geq 0$). Cases (a)–(c) show the effect of alignment and attraction on the stability of the steady states, whereas cases (d)–(f) show the effect of total population size and attraction on this stability. The value of the turning rates is the same for all cases. The threshold values Q^*, Q^{**}, A^*, and A^{**} determine the number of spatially homogeneous steady states. However, the stability of these steady states is greatly influenced by attraction and, not shown here, by the turning rates. One can see that an increase in the magnitude of attraction from $q_{\rm a} = 0.1$ for (a) and (d) to $q_{\rm a} = 10$ for (c) and (f), leads to an increase in the parameter range (A and $q_{\rm al}$) for the unstable steady states. If we look at the total population size, for instance, these results suggest that unless there is a very strong attraction, large number of individuals do not aggregate. Therefore, we conclude that both alignment and total population size have similar qualitative effects on the number of steady states (Fig. 5(c)) as well as their stability (Fig. 7).

We should also note that for small attraction ($q_{\rm a} \leq q_{\rm r}$) and large turning rates, it is possible to have a hysteresis phenomenon (Fig. 7(a) and (d)). More precisely, if we start for example with a very small $q_{\rm al}$, then the only possible steady state is

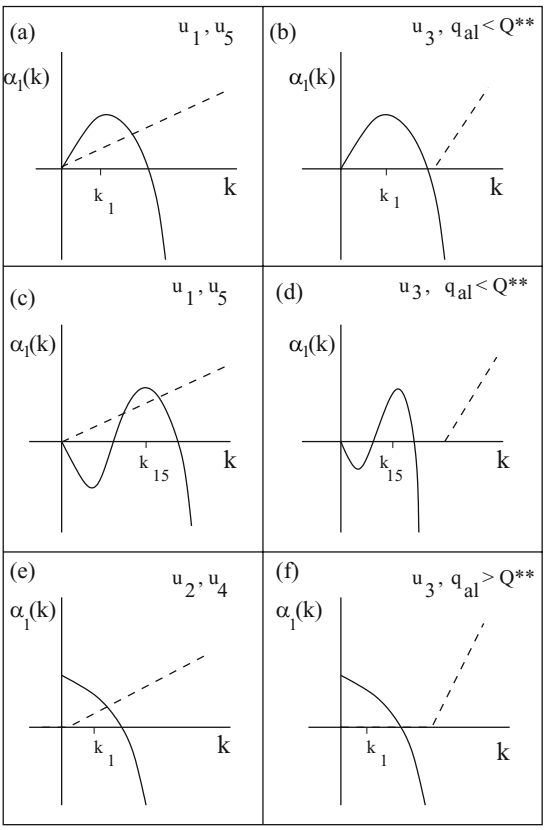

Fig. 6 Examples of dispersion relations $\alpha_1(k)$ for the system, represented by Eq. (1). The *solid curve* represents $\mathrm{Re}(\alpha_1(k))$, while the *dashed curve* represents $\mathrm{Im}(\alpha_1(k))$. For cases (a), (c), and (e), $\mathrm{Im}(\alpha_1(k_c)) \neq 0$, while for (b), (d), and (f), $\mathrm{Im}(\alpha_1(k_c)) = 0$, where k_c is the critical wavenumber that emerges (shown is $k_c = k_1$ for (a), (b), (e), and (f), and $k_c = k_{15}$ for (c) and (d)). Note that $\mathrm{Im}(\alpha_1(k_c)) = 0$ only for u_3^*. Cases (a) and (b) are obtained for small turning rates and large q_a, while (c) and (d) are for large turning rates, and relatively small q_a. Cases (e) and (f) are obtained for $q_{al} \in (Q^*, Q^{**})$ and $u_{2,4}^*$, or for $q_{al} > Q^{**}$ and u_3^*.

(u_3^*, u_3^*), and it is stable. As we increase alignment, this state will lose stability at $q_{al} = Q^{**}$ (Fig. 7(a)). Depending on initial conditions, the system will choose one of the two other solutions: (u_1^*, u_5^*) or (u_5^*, u_1^*), both of which are stable. However, if we now decrease the alignment beyond Q^{**}, the system will not return immediately to (u_3^*, u_3^*). It will return later, when u_1^* and u_5^* lose stability at Q^*. A similar phenomenon is observed when increasing and decreasing the total population size A.

3.3. The effect of different interaction ranges on group formation

We now use the dispersion relation, represented by Eq. (24), to study the effect of the three interaction ranges, s_r, s_{al}, and s_a on group formation. We investigate

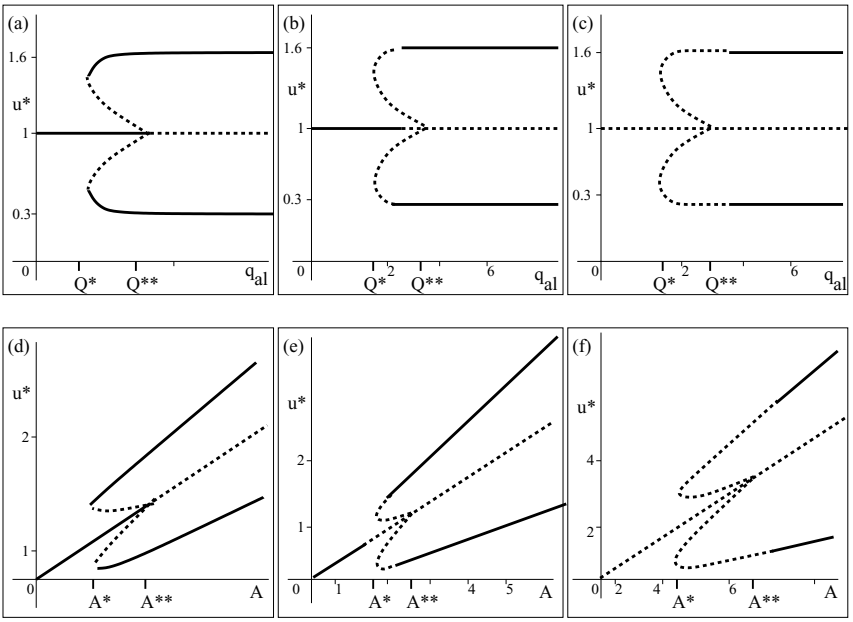

Fig. 7 Spatially homogeneous steady states and their stability, as interindividual attraction, q_a, increases: (a)–(c) show bifurcations in the (q_{al},u) plane, while (d)–(f) show bifurcations in the (A, u) plane. *Solid curves* represent the stable steady states, while the *dotted curves* represent the unstable steady states, as given by $\mathrm{Re}(\alpha_1(k_1)) \geq 0$. The magnitude of attraction is increased from $q_a = 0.1$ for (a) and (d), to $q_a = 2$ for (b) and $q_a = 1$ for (e), and to $q_a = 10$ for both (c) and (f). As a result, the parameter range for the unstable steady states (i.e., the *dotted curve*) is also increasing.

the stability of the spatially homogeneous steady state (u_3^*, u_3^*) by increasing (or decreasing) the size of these ranges while keeping all other parameters constant. At the end, we will briefly discuss the effect of these ranges on the stability of u_i^*, $i = 1, 2, 4, 5$. It should be mentioned that if for some i we have $\mathrm{Re}(\alpha(k_i)) > 0$, while for all other $j \neq i$ we find $\mathrm{Re}(\alpha(k_j)) < 0$, then the linear analysis predicts that i groups will emerge.

If we graph the dispersion relation, we see that an increase in the repulsion range, s_r, while keeping everything else constant, leads to the stability of u_3^* (Fig. 8(a)). Increasing it even further would lead to the biologically unrealistic situation $s_r > s_a$. For alignment (Fig. 8(b)), the results are similar to those obtained for the repulsion case.

If we increase the attraction range, the dispersion relation shows a translation to the left of the wavenumber that becomes unstable (Fig. 8(c)). For example, suppose k_2 is the unstable wavenumber initially (correspondingly, there are two groups). After increasing the attraction range, k_1 is the unstable wavenumber (correspondingly, there is one group). Biologically, this makes sense since when s_a is increased, individuals perceive information over larger distances. Two separate groups now can sense each other and merge.

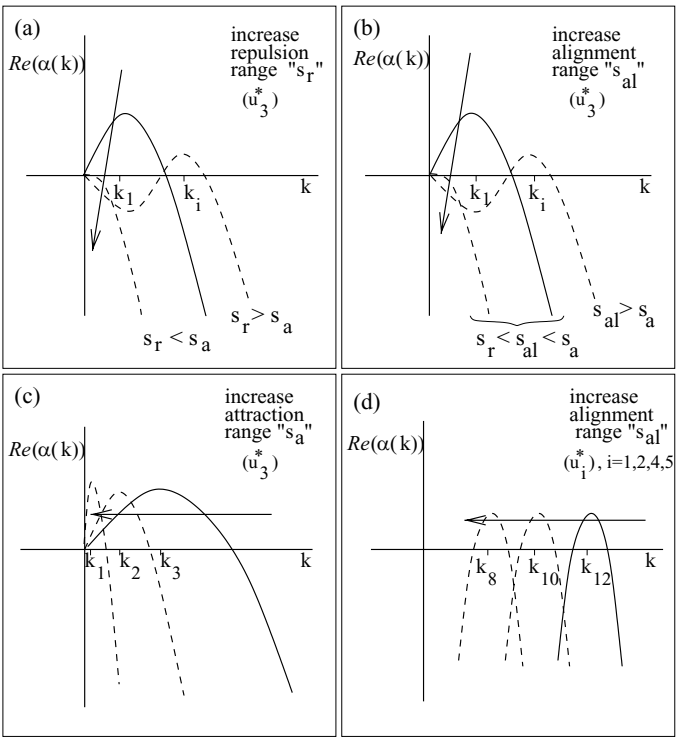

Fig. 8 The effect of the interaction ranges s_r, s_{al}, and s_a, on the local stability of homogeneous steady states u_i^*, $i = 1..5$. The plots show $\mathrm{Re}(\alpha_1(k))$. The *arrows* show what happens with the graph of $\mathrm{Re}(\alpha_1)$ as we increase the interaction ranges. For u_3^*, an increase in the repulsion range (case (a)) or the alignment range (case (b)) leads to stability of the steady state. For example, for case (a), let us assume that initially the mode that emerges is the one with the wavenumber k_1. As we increase the repulsion range s_r, making sure at the same time that $s_r < s_a$, we see that this mode becomes stable ($\mathrm{Re}(\alpha_1(k_1)) < 0$). Increasing s_r even more (i.e., $s_r > s_a$), the mode that emerges is the one with the wavenumber k_i, $i > 1$. A similar explanation holds for (b). An increase in the attraction range (case (c)) results in a shift to the left of the wavenumber that will emerge. For u_i^*, $i = 1, 2, 4, 5$, an increase in the alignment range leads to the same shift to the left (case (d)).

The stability of the other four steady states u_i^*, $i = 1, 2, 4, 5$, does not seem to be influenced significantly by alterations in the size of the attraction or repulsion ranges. More precisely, neither the location nor the amplitude of the leading eigenmode varies much as the corresponding interaction ranges s_a and s_r vary. However, an increase in the alignment range results in a translation to the left of the wavenumber that emerges (Fig. 8(d)). This means that when there are more individuals moving in one direction than the other (i.e., the steady states (u^*, u^{**}) with $u^* \neq u^{**}$), the attempt to match one's movement direction to the movement direction of those neighbors that are farther away, causes small groups of individuals to come together and form larger aggregations.

4. Numerical results

To have a better idea about the rich behavior of the system, represented by Eq. (1), we investigate the spatially nonhomogeneous solutions numerically, using a first-order upwind scheme (e.g., LeVeque (1992)) with periodic boundary conditions. The infinite integrals, represented by Eqs. (5)–(8) were approximated by integrals on finite domains: $0 < x < 6i$, $i = s_r, s_a$, for attractive and repulsive kernels, and $0 < x < 2s_{al}$ for alignment. These finite integrals were further discretized using Simpson's method. The kernels used for these simulations are described by Eqs. (9) and (11). To check the validity of our results obtained via linear stability analysis, we choose the initial conditions to be small random perturbations of the spatially homogeneous steady states. The parameters for the domain length and interaction ranges are chosen to be $L = 10$, $s_r = 0.25$, $s_{al} = 0.5$, and $s_a = 1$. These four parameters, as well as y_0, m_{al}, m_a, m_r, and A, are kept fixed during the simulations (see Table 1). All other parameters will be varied at some point. The parameters that are varied are precisely those that can be used to characterize animal groups during different behaviors.

To make sure that the boundary conditions do not lead to artifacts as a result of the interactions of the front of the wave with its back, we compared the results to simulations on larger domains up to $L = 20$, and found no measurable difference in the results.

Numerical simulations show four types of possible behavior: stationary pulses, traveling pulses, traveling trains, and zigzag pulses (Figs. 9 and 10). By stationary pulses (Fig. 9(a) and (d)), we mean spatially nonhomogeneous steady states. Traveling pulses (Fig. 9(b)) are defined as spatially nonhomogeneous solutions that have a fixed shape and move at a constant speed c: $u^{\pm}(x,t) = U^{\pm}(z)$, $z = x - ct$, and $U^{\pm}(\pm\infty) = 0$. The periodic boundary conditions allow us to treat the domain as infinite, and, therefore, it makes sense to consider traveling pulses. Traveling trains (Fig. 9(c)) are periodic solutions of the form $u^{\pm}(x,t) = U^{\pm}(z)$, $z = x - ct$, with $U^{\pm}$ periodic functions of z. The zigzag pulses (Fig. 10) are traveling solutions that periodically change direction. Moreover, compared to the case of traveling pulses, where the shape of solutions does not change, for zigzag pulses the shape changes slightly when the entire group turns around.

A first observation is that both stationary and moving groups have clearly defined boundaries, where the population density drops to zero very quickly. Moreover, in the case of moving groups (Fig. 9(b)), the profile is steeper at the leading edge of the group, and shallower at the back. This phenomenon is caused by attraction toward other individuals. Under the influence of the attractive force, organisms at the front of the group have the tendency to turn around more often, to stay in contact with the others. Therefore, they move slower than those at the rear of the group, and this leads to crowding at the leading edge of the group.

In what follows, we present the results in three separate cases: a case that contains only attraction and repulsion, a case with only alignment, and a case that takes into consideration all three social interactions. The types of solutions that can be obtained in each of these cases are summarized in Table 2 and discussed

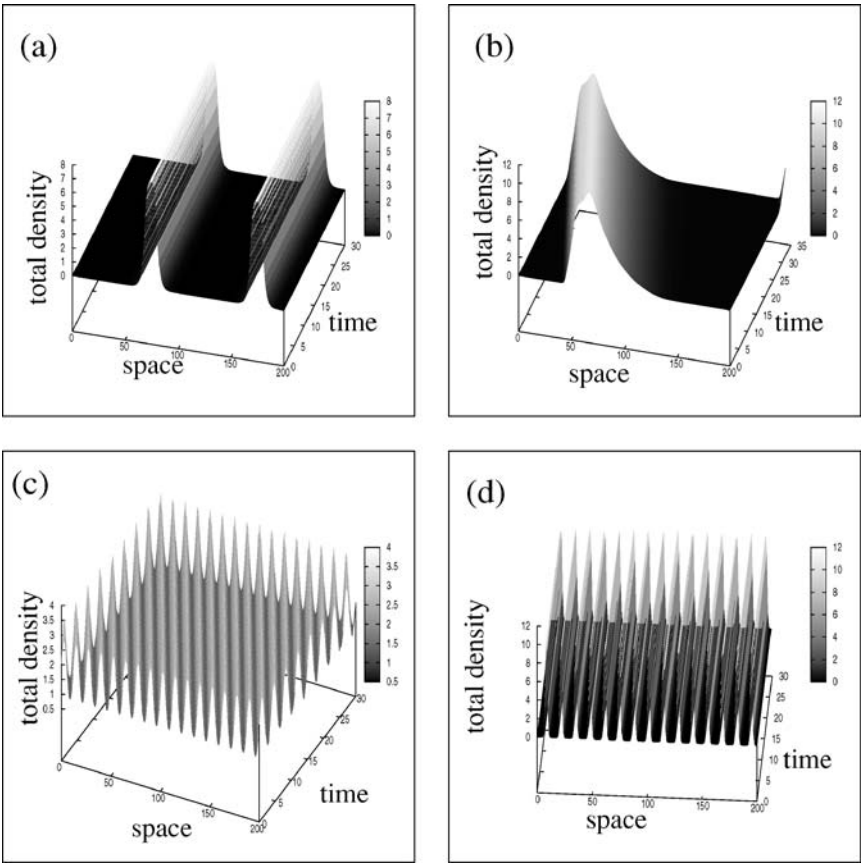

Fig. 9 Examples of long-time behavior: (a) Stationary pulses obtained for $q_a > q_r$ and no alignment: $q_a = 10, q_r = 0.1, q_{al} = 0, \gamma = 0.1, \lambda_1 = 0.2, \lambda_2 = 0.9$; (b) Traveling pulse: $q_a = 5.2, q_r = 0.1, q_{al} = 2.8, \gamma = 0.1, \lambda_1 = 0.2, \lambda_2 = 0.9$; (c) Traveling trains obtained for $q_{al} = 2.1, q_a = 0, q_r = 0, \gamma = 0.1, \lambda_1 = 0.4, \lambda_2 = 1.8$; (d) Stationary pulses, obtained for $q_{al} = 2, q_a = 0, q_r = 0, \gamma = 0.1, \lambda_1 = 1.33, \lambda_2 = 6$.

later. These results were simulated with fixed parameters sampled from the ranges described by Table 1.

(i) *Only attraction and repulsion.* For $q_{al} = 0$, the only possible spatially homogeneous solution is $(u^+, u^-) = (u_3^*, u_3^*)$ (Fig. 5). In the parameter range where it is unstable, if we start with small random perturbations of this steady state as initial conditions, we obtain stationary pulses (Fig. 9(a)). We have sampled a large number of parameter combinations (from the parameter space where u_3 is unstable), and the results always showed stationary pulses. These results suggest that attraction and repulsion are sufficient to cause group formation, but not sufficient to make the group travel.

(ii) *Only alignment.* When alignment is the only social force considered, it is possible to have up to five spatially homogeneous solutions $(u_i^*, i = 1..5)$ (Fig. 5).

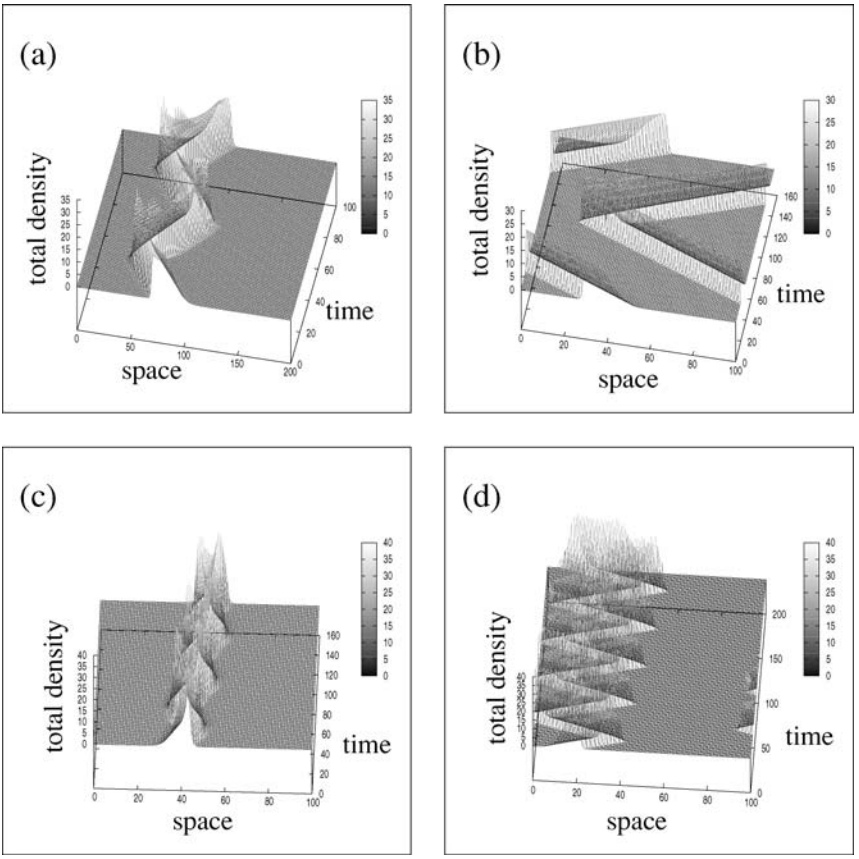

Fig. 10 Zigzag movement is obtained when $q_a \gg q_r$. Cases (a) and (b) show the symmetric pattern that arises as $p_r = p_l$, while cases (c) and (d) show the biased random movement that arises when this symmetry is broken, i.e., $p_r \neq p_l$. The following parameters are the same for all these four cases: $q_r = 1.2$, $q_a = 15.0$, $q_{al} = 2.0$, $\gamma = 0.1$. The turning rates are as follows: for (a) and (c) $\lambda_1 = 0.2$, and $\lambda_2 = 0.9$; for (b) $\lambda_1 = 0.33$, $\lambda_2 = 1.5$; for (d) $\lambda_1 = 0.4$, $\lambda_2 = 1.8$.

Locally unstable steady states (Fig. 6(c) and (d)) are possible when the turning rates are large, and these solutions evolve into either traveling trains (Fig. 9(c)) or stationary pulses (Fig. 9(d)). More precisely, traveling trains are possible when the initial conditions are perturbations of $(u^+, u^-) = (u_1^*, u_5^*)$, whereas stationary pulses are obtained when we start either with perturbations of (u_3^*, u_3^*), or with perturbations of (u_1^*, u_5^*) and very large turning rates.

(iii) *Attraction, repulsion, and alignment.* The most complex behavior is obtained when all three social interactions take place. In addition to the behaviors described above, we also observe zigzag pulses in this case (Fig. 10(a)–(d)). This behavior is caused by high interindividual attraction ($q_a \gg q_r$). If organisms weigh the information received from the left or right equally ($p_r = p_l$), then

Table 2 A summary of the different types of possible solutions exhibited by the model under the influence of three different sets of social interactions: traveling trains, traveling pulses, stationary pulses, and zigzag pulses

Case	Social interactions	Traveling trains	Traveling pulses	Stationary pulses	Zigzag pulses
(i)	Only attraction and repulsion	No	No	Yes	No
(ii)	Only alignment	Yes	No	Yes	No
(iii)	Attraction, repulsion, and alignment	Yes	Yes	Yes	Yes

the zigzag paths are symmetric (i.e., the length of the right moving path is the same as the length of the left moving path), as shown in Fig. 10(a) and (b). Moreover, if $p_r \neq p_l$, the symmetry is broken and this causes a bias in the movement (Fig. 10(c) and (d)).

We observe that the lengths of the paths in the zigzag movement are correlated with the turning rates, λ_1 and λ_2. For Fig. 10(a) and (c), the turning rates are small (i.e., $\lambda_1 = 0.2, \lambda_2 = 0.9$) and we observe short path lengths. In contrast, when we increase the turning rates (e.g., $\lambda_1 = 0.4$, $\lambda_2 = 1.8$), we observe longer path lengths, as shown in Fig. 10(b) and (d). The explanation for this is that when these rates are small, the individuals in the middle part of the group as well as those at the back do not turn very often. However, due to large attraction, those at the front of the group turn around to make sure they are still with the rest of the group. This leads to a steep increase in the number of individuals at the leading edge of the group that move in the opposite direction. As a result, the entire group turns around. However, when the turning rates are large, the straight paths between group turning maneuvers are much longer. The individual turns help organisms to move away from their neighbors and keep them well spaced for a longer time.

Another important aspect of the zigzag movement that should be mentioned is the structure of the turn. Figure 11 shows two types of group behavior that can be observed during the turning maneuver. Small turning rates (Fig. 11(a)), lead to a very compact group *during* the turns, while large turning rates (Fig. 11(b)), make the group more compact *before* the turning maneuver, but less compact during and after the turn.

Zigzag movement can be understood to be a transitory type of behavior between traveling pulses, obtained when attraction is small, and stationary pulses, obtained when attraction is extremely large compared to repulsion, as shown in Fig. 12. If we increase attraction, the model shows a transition from one type of solution to another. For attraction taking small to medium values compared to repulsion, the system displays traveling pulses (as in Fig. 9(b)). As the magnitude of attraction increases, these groups start moving back and forth, in a zigzag manner (as in Fig. 10). When this social interaction becomes extremely strong (for example, $q_a = 20$, and $q_r = 0.1$, and all other parameters as specified in Fig. 10), the aggregations become stationary.

A similar transitory type of behavior can be obtained when varying multiple parameters. For example, the model could be used to describe the succession of

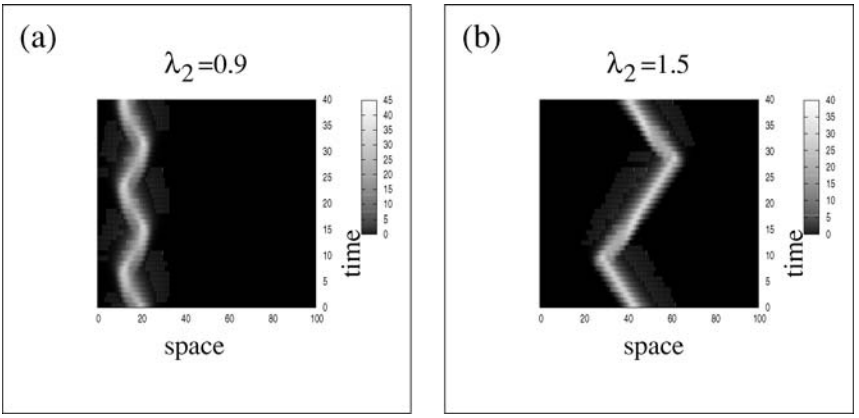

Fig. 11 The structure of a turn during zigzag movement is determined by the turning rates: (a) $\lambda_1 = 0.2$, $\lambda_2 = 0.9$; (b) $\lambda_1 = 0.33$, $\lambda_2 = 1.5$. The brighter the color, the higher the population density. For small individual turning rates, the density is higher *during* the turn (i.e., the group is more compact), while for large individual turning rates (especially for large λ_2), the density is higher *between* the turns.

daily activity patterns exhibited by different groups of animals. Usually, these transitions from one activity to another can be influenced by internal factors (e.g., hunger, necessity to rest, etc.), or external ones (e.g., temperature (Uvarov, 1966) or light (Helfman, 1993)). These factors have an impact on group parameters, such as motility, and this translates into different turning rates and speeds (Uvarov, 1966).

To exemplify this transitional process, we look at the following succession of activities: forage → rest → travel → forage. The initial conditions for forage are random perturbations of spatially homogeneous steady state (u_1^*, u_5^*). For the next three activities, the initial conditions for the simulations are the densities generated by the previous activity. Table 3 summarizes possible relative magnitudes for model parameters.

Figure 13 shows the outcomes of numerical simulations that describe these activities. Initially, there are many small clusters that travel for a while, and then stop. During the resting period, the groups are stationary, with the peak of total local densities decreasing. However, as both attraction and alignment increase to

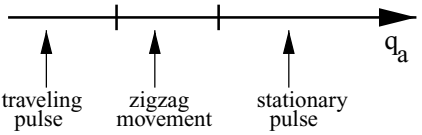

Fig. 12 An illustration of the possible types of solutions and the transitions between them as one varies the attraction parameter q_a. Initially, there is a traveling pulse, and as attraction increases, it starts moving in a zigzag manner. A very large attraction force keeps all individuals together, hindering the group movement.

Table 3 Examples of magnitudes of model parameters that characterize animal behavior corresponding to different activities

Activity	γ	λ_1, λ_2	q_{al}	q_r	q_a
Traveling	Large	Small	Large	Small	Large
Foraging	Medium, large	Large	Medium	Large	Small
Rest	Small	Medium	Small	Medium	Medium

simulate travel, all animals gather into one large aggregation, which moves toward a new site. Once having arrived there, parameters are changed to simulate foraging and the group spreads again. It should be noted that even though we use the same parameters to simulate the two foraging behaviors, the initial conditions play a very important role. Initially, the small groups that form during foraging are moving through the domain. When we change the parameters from travel back to foraging, the groups that arise are now stationary. A similar hysteresis phenomenon was obtained by Couzin et al. (2002), with a Lagrangian model.

All the numerical results presented here were obtained using odd kernels for attraction and repulsion, and a translated Gaussian kernel for alignment (Fig. 4(b)). We also ran simulations using translated Gaussian kernels for all types

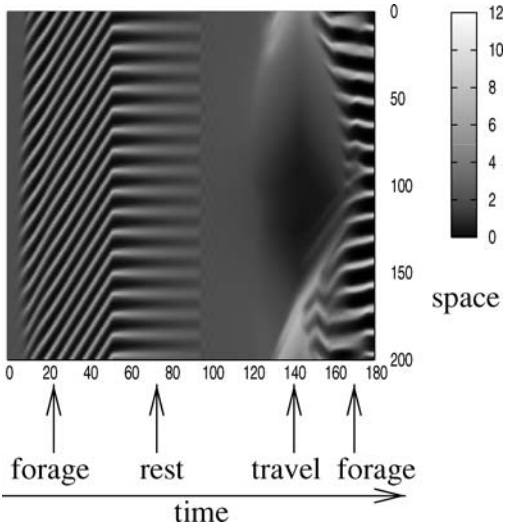

Fig. 13 The figure shows a "bird's eye view" for the total population density during the succession of three activities: forage → rest → travel → forage. The lighter the color, the higher the population density. Parameter values are chosen in accordance with Table 3. During foraging ($q_r = 2.0$, $q_a = 0.1$, $q_{al} = 1.9$, $\gamma = 0.089$, $\lambda_1 = 1.3$, $\lambda_2 = 6$), individuals turn frequently and attraction is smaller than repulsion, which leads to many small groups moving around the domain. During rest ($q_r = 0.10$, $q_a = 2.1$, $q_{al} = 0.5$, $\gamma = 0.015$, $\lambda_1 = 0.286$, $\lambda_2 = 1.286$), the individuals slow down and turn less frequently. The groups have now a tendency to disperse. To travel ($q_r = 0.5$, $q_a = 4.1$, $q_{al} = 2.0$, $\gamma = 0.1$, $\lambda_1 = 0.2$, $\lambda_2 = 0.9$), the attraction increases and all the individuals come together to form one large group that moves around the domain. To forage again, the group splits into multiple small groups that spread over the domain.

of interactions (attraction, repulsion, and alignment) (Fig. 4(a)), and the results showed similar qualitative behavior for the solutions.

It was previously shown (Grünbaum, 1998; Gazi and Passino, 2002) that group polarization helps populations to improve their searching behavior, by climbing noisy gradients faster. Our model shows that without alignment and in the absence of external environmental cues, group movement does not occur. Mathematical proof of this result is the subject of a forthcoming paper where we look at the possible types of solution when repulsion and attraction are the only social interactions. Group movement is possible with alignment, but it depends on the magnitude of the turning rates: high individual turning rates make it impossible for the group to move as an entity. Therefore, we can say that alignment appears to be a necessary ingredient, but not a sufficient one for group movement.

In conclusion, the model shows that interactions between different social factors give rise to a wide range of patterns. We have seen, for example, that medium attraction combined with repulsion and alignment leads to traveling pulses, while large attraction plus repulsion and alignment leads to zigzag pulses. None of these two types of solutions can be obtained with alignment alone, nor with attraction and repulsion alone. They are the result of all three social interactions.

5. Parallels to biology

In this section, we discuss how the complex patterns that emerge in the model above relate to observations in nature.

We begin by analyzing the shape of the aggregations. We saw before that groups are well defined, i.e., the density outside the group is essentially zero. Moreover, our results show an increased density at the leading edge of the moving groups, due to leading individuals turning around to return to the group under the influence of attraction forces. These results seem to agree with empirical studies (Uvarov, 1966; Bumann and Krause, 1993). Uvarov (1966), observes that "a noticeable feature of a band marching in frontal formation is the greater density of hoppers at its leading edge," a possible explanation for this being that "the leading hoppers may hesitate because there are no other hoppers in their anterior field of vision and they may even return to the front after jumping beyond it; the hoppers behind are, therefore, likely to catch up with the moving front causing a concentration" (vol. II, p. 164).

Focusing now on the four types of spatial patterns displayed by our model, we observe that traveling pulses and stationary pulses correspond to moving (e.g., traveling schools of fish, flocks of birds) and stationary (e.g., resting) groups of animals. Uvarov (1966) describes the aggregative behavior of basking locusts that form ground groups in the morning or in the evening, when the temperature is low and activity ceases.

Uvarov (1966) also offers an illustrating example of oscillations (i.e., traveling trains) exhibited by animal groups. Commenting on the interindividual

interactions of locust hoppers, Uvarov describes how "a jump by a disturbed hopper leads to an outburst by others; this spreads through the group or band, and eventually subsides in a way reminiscent of ripples on the surface of water caused by a pebble"(vol. II, pp. 165). Other examples can be observed in some bird flocks (Buchanan et al., 1988) or fish schools (Radakov, 1973).

Zigzag movement is seen in flocks of birds (Humphries and Driver, 1970; Davis, 1980; Buchanan et al., 1988) that rapidly change direction, making sharp turns of 180° (Davis, 1980). Potts (1984) observed that birds do not turn simultaneously, but the maneuver is initiated by birds banking toward the flock, and not by those that turn away from the flock. The movement then propagates like a wave throughout the flock. However, Davis (1980) suggested that some birds may signal their intention to change direction, and when a certain number of birds make the same decision, the entire flock turns.

The empirical results also differentiate between two types of group structure during the turning behavior. Studying the turning behavior in Rock Dove flocks, Pomeroy and Heppner (1992) noticed that the flock became more compact just before turning, and then it expanded. They also pointed out that this type of turning is different from what is observed in fish, where groups are usually compact, and they expand as they make a turn. Moreover, the authors suggested that this difference may be explained by the interindividual distances that are smaller in fish schools, compared to those in bird flocks. Partridge et al. (1980) discussed the relationship between the interindividual distance in fish schools, and the fish body structure that causes the maneuverability of individuals. They noticed that the fish that are more maneuverable (such as cod and saithe) have smaller interindividual distances, whereas a "stiff-bodied" fish (such as herring) has larger interindividual distances.

As we have previously seen, our mathematical model shows the same two types of group structures during the turning behavior. The mechanisms that determine these types of group structures are the different individual turning rates exhibited by animals. Consequently, the model suggests that it might be possible to explain the two types of group structures in terms of individual turning rates. These results show that there is need for a more indepth analysis that correlates the compactness of the observed aggregations with the individual turning rates.

While the biological patterns we described here are complex two- and three-dimensional phenomena, the simulation results show that our one-dimensional model nonetheless captures essential features of these patterns.

6. Conclusions

The goal of this paper was to derive and analyze a general one-dimensional mathematical model for the study of group formation in self-organizing communities of organisms. We focused on a hyperbolic model of conservation laws and, following Pfistner's approach (Pfistner, 1990), incorporated attraction, repulsion, and alignment into the turning rates. The way these social interactions were incorporated depended on some assumptions that we made about animal communication.

We also assumed that an organism changes its movement direction only after weighing the information received from left and right. The social interactions were thus defined in terms of communication and distances, and not just distance alone.

One-dimensional models for group formation and movement usually describe one type of behavior at a time. For example, Pfistner (1995) reported aggregations, Mogilner and Edelstein-Keshet (1999) reported traveling waves. The hyperbolic model presented in this paper not only reports both stationary and traveling waves, but also traveling trains and zigzag pulses.

Numerical simulations showed that incorporating attraction and repulsion alone can only lead to stationary groups. Depending on the magnitude of attraction and frequency of turning, there is either one large aggregation, or many small clusters. However, alignment alone leads to the formation of a large number of small groups that can either travel or be stationary. Moreover, the results reveal that in the absence of external cues, alignment is a necessary ingredient for the groups to move. The most complex types of behavior observed in biological systems can be explained only as a result of the interactions between all these social forces. In this case, it is possible to obtain not only the classical types of solutions (i.e., traveling trains and pulses, and stationary pulses), but also a new kind of long-time behavior: zigzag pulses. These solutions apparently emerge as a result of interactions between alignment, repulsion, and large attraction.

Also, we have studied the transitions between different daily activities, as the model parameters are varied. To our knowledge, this is the first continuum model that looks at the transition between different activities exhibited by animal groups. Similar transition results were previously obtained with an individual-based model (Couzin et al., 2002).

Linear analysis and numerical simulations both suggest that there is an intermediate range of values for the parameter describing the magnitude of the alignment, or for the total population size, for which population clusters can form.

The length scale of the interaction ranges also plays an important role in self-organization, as shown by analyzing the stability of the spatially homogeneous steady states.

In this paper, we have restricted ourselves to one spatial dimension. In nature, the majority of biological aggregations are in two or three dimensions. However, the model demonstrates a straightforward way to model interactions based on animal communication. The model, as written, is general, and would need to be specifically tailored to describe a particular organism. By changing the way we model communication (i.e., the way we model how organisms receive the stimuli: from both directions, or only from one direction), the mathematical model can easily be adapted to a particular species.

The one-dimensional model can approximate the behavior of animal groups in higher dimensions if they move in a domain that is much longer than wide. Also, this approximation may be acceptable in the case of directional communication (e.g., vision). However, for a more realistic and general case, the model should be extended to two spatial dimensions. This is a subject for future research.

Appendix A

Here we show that for $L \to \infty$, $\hat{\Gamma_j}(k)$ can be approximated by $\hat{K_j}(k)$, where $j \in \{\mathrm{r}, \mathrm{al}, \mathrm{a}\}$.

$$\lim_{L\to\infty} \int_{-L/2}^{L/2} \Gamma_j(s) \mathrm{e}^{\pm \mathrm{i}ks}\, \mathrm{d}s = \lim_{L\to\infty} \int_{-L/2}^{L/2} \left(\sum_{n=-\infty}^{n=-1} K_j(s+nL) + K_j(s) + \sum_{n=1}^{\infty} K_j(s+nL) \right) \mathrm{e}^{\pm \mathrm{i}ks}\, \mathrm{d}s = \lim_{L\to\infty} \int_{-L/2}^{L/2} K_j(s) \mathrm{e}^{\pm \mathrm{i}ks}\, \mathrm{d}s + \lim_{L\to\infty} \int_{-L/2}^{L/2} \left(\sum_{n=-\infty}^{n=-1} K_j(s+nL) + \sum_{n=1}^{n=\infty} K_j(s+nL) \right) \mathrm{e}^{\pm \mathrm{i}ks}\, \mathrm{d}s$$

where the kernels are assumed to decrease exponentially as $L \to \infty$ (see Eqs. (9) and (11)). For large L, the terms containing the sums are approaching zero and, therefore,

$$\lim_{L\to\infty} \int_{-L/2}^{L/2} \Gamma_j(s) \mathrm{e}^{\pm \mathrm{i}ks}\, \mathrm{d}s = \hat{K_j}^{\pm}(k). \tag{A.1}$$

Appendix B

The full model used for the linear stability analysis and the numerical simulations is described by:

$$\begin{aligned}
\partial_t u^+(x,t) + \partial_x(\gamma u^+(x,t)) &= -(\lambda_0 + \lambda_2 0.5 \tanh(y^+[u^+,u^-] - y_0))u^+(x,t) \\
&\quad + (\lambda_0 + \lambda_2 0.5 \tanh(y^-[u^+,u^-] - y_0))u^-(x,t), \\
\partial_t u^-(x,t) - \partial_x(\gamma u^-(x,t)) &= (\lambda_0 + \lambda_2 0.5 \tanh(y^+[u^+,u^-] - y_0))u^+(x,t) \\
&\quad - (\lambda_0 + \lambda_2 0.5 \tanh(y^-[u^+,u^-] - y_0))u^-(x,t), \\
u^{\pm}(x,0) &= u_0^{\pm}(x), x \in \mathbf{R},
\end{aligned} \tag{B.1}$$

with $\lambda_0 = \lambda_1 + 0.5\lambda_2$, and $y^{\pm}[u^+, u^-]$ given by

$$\begin{aligned}
y^{\pm}[u^+,u^-] = q_{\mathrm{r}} &\int_{-\infty}^{\infty} K_{\mathrm{r}}(s) u(x \pm s)\, \mathrm{d}s \\
&- q_{\mathrm{a}} \int_{-\infty}^{\infty} K_{\mathrm{a}}(s) u(x \pm s)\, \mathrm{d}s \\
&+ q_{\mathrm{al}} \int_{0}^{\infty} K_{\mathrm{al}}(s) \left(u^{\mp}(x \pm s) - u^{\pm}(x \mp s) \right)\, \mathrm{d}s.
\end{aligned}$$

Acknowledgements

RE acknowledges support from a University of Alberta FS Chia Scholarship. GdeV acknowledges partial support from an NSERC Discovery Grant. MAL acknowledges support from an NSERC Discovery Grant and Canada Research Chair. FL acknowledges support from the Pacific Institute for the Mathematical Sciences as a Postdoctoral Fellow.

References

Beecham, J.A., Farnsworth, K.D., 1999. Animal group forces resulting from predator avoidance and competition minimization. J. Theor. Biol. 198, 533–548.
Breder, C.M., 1954. Equations descriptive of fish schools and other animal aggregations. Ecology 35, 361–370.
Bressloff, P.C., 2004. Euclidean shift-twist symmetry in population models of self-aligning objects. SIAM J. Appl. Math. 64, 1668–1690.
Buchanan, J.B., Schick, C.T., Brennan, L.A., Herman, S.G., 1988. Merlin predation on wintering dunlins: Hunting success and dunlin escape tactics. Wilson Bull. 100, 108–118.
Bumann, D., Krause, J., 1993. Front individuals lead in shoals of three-spined sticklebacks (*Gasterosteus aculeatus*) and juvenile roach (*Rutilus rutilus*). Behaviour 125, 189–198.
Couzin, I.D., Krause, J., James, R., Ruxton, G.D., Franks, N.R., 2002. Collective memory and spatial sorting in animal groups. J. Theor. Biol. 218, 1–11.
Davis, M., 1980. The coordinated aerobatics of dunlin flocks. Anim. Behav. 28, 668–673.
Edelstein-Keshet, L., Watmough, J., Grünbaum, D., 1998. Do travelling band solutions describe cohesive swarms? An investigation for migratory locusts. J. Math. Biol. 36(6), 515–549.
Flierl, G., Grünbaum, D., Levin, S., Olson, D., 1999. From individuals to aggregations: The interplay between behavior and physics. J. Theor. Biol. 196, 397–454.
Gazi, V., Passino, K.M., 2002. Stability analysis of swarms. In: Proc. Am. Control Conf. Anchorage, AK, pp. 8–10.
Grünbaum, D., 1998. Schooling as a strategy for taxis in a noisy environment. Evol. Ecol. 12, 503–522.
Gueron, S., Levin, S.A., Rubenstein, D.I., 1996. The dynamics of herds: From individuals to aggregations. J. Theor. Biol. 182, 85–98.
Helfman, G., 1993. Fish behaviour by day, night and twilight. In: Pitcher, T. (Ed.), Behaviour of Teleost Fishes. Chapman & Hall, London, pp. 479–512.
Humphries, D.A., Driver, P.M., 1970. Protean defence by prey animals. Oecologia (Berl.) 5, 285–302.
Huth, A., Wissel, C., 1994. The simulation of fish schools in comparison with experimental data. Ecol. Model. 75/76, 135–145.
Kac, M., 1974. A stochastic model related to the telegrapher's equation. Rocky Mt. J. Math. 4, 497–509.
Kerner, B.S., Konhäuser, P., 1994. Structure and parameters of clusters in traffic flow. Phys. Rev. E 50, 54–83.
Kube, C.R., Zhang, H., 1993. Collective robotics: From social insects to robots. Adapt. Behav. 2, 189–218.
LeVeque, R., 1992. Numerical Methods for Conservation Laws. Birkhäuser, Basel, Switzerland.
Lutscher, F., 2002. Modeling alignment and movement of animals and cells. J. Math. Biol. 45, 234–260.
Lutscher, F., Stevens, A., 2002. Emerging patterns in a hyperbolic model for locally interacting cell systems. J. Nonlinear Sci. 12, 619–640.
Marler, P., 1967. Animal communication signals. Science 157, 769–774.
Mogilner, A., Edelstein-Keshet, L., 1996. Spatio-angular order in populations of self-aligning objects: Formation of oriented patches. Physica D 89, 346–367.
Mogilner, A., Edelstein-Keshet, L., 1999. A non-local model for a swarm. J. Math. Biol. 38, 534–570.

Mogilner, A., Edelstein-Keshet, L., Bent, L., Spiros, A., 2003. Mutual interactions, potentials, and individual distance in a social aggregation. J. Math. Biol. 47, 353–389.
Okubo, A., 1986. Dynamical aspects of animal grouping: Swarms, school, flocks and herds In: Kotani, M. (Ed.). Adv. Biophys. 22, 1–94.
Okubo, A., Grünbaum, D., Edelstein-Keshet, L., 2001. The dynamics of animal grouping. In: Okubo, A., Levin, S. (Eds.), Diffusion and Ecological Problems: Modern Perspectives. Springer, New York, pp. 197–237.
Othmer, H.G., Dunbar, S.R., Alt, W., 1988. Models of dispersal in biological systems. J. Math. Biol. 26, 263–298.
Parrish, J.K., 1999. Using behavior and ecology to exploit schooling fishes. Environ. Biol. Fish. 55, 157–181.
Partan, S.R., Marler, P., 2005. Issues in the classification of multimodal communication signals. Am. Nat. 166, 231–245.
Partridge, B.L., Pitcher, T., Cullen, J.M., Wilson, J., 1980. The three-dimensional structure of fish schools. Behav. Ecol. Sociobiol. 6, 277–288.
Pfistner, B., 1990. A one dimensional model for the swarming behavior of Myxobakteria. In: Alt, W., Hoffmann, G. (Eds.), Biological Motion, Lecture Notes on Biomathematics, vol. 89. Springer, New York, pp. 556–563.
Pfistner, B., 1995. Simulation of the dynamics of myxobacteria swarms based on a one-dimensional interaction model. J. Biol. Syst. 3, 579–588.
Pomeroy, H., Heppner, F., 1992. Structure of turning in airborne rock dove (*Columba Livia*) flocks. The Auk 109, 256–267.
Potts, W.K., 1984. The chorus-line hypothesis of manoeuvre coordination in avian flocks. Nature 309, 344–345.
Radakov, D.V., 1973. Schooling in the Ecology of Fish. Wiley, New York.
Reuter, H., Breckling, B., 1994. Self organization of fish schools: An object-oriented model. Ecol. Model. 75/76, 147–159.
Reynolds, C.W., 1987. Flocks, herds and schools: A distributed behavioral model. Comput. Graph. 21, 25–34.
Robbins, T., 2003. Seed dispersal and biological invasion: A mathematical analysis. PhD thesis, University of Utah.
Segel, L.A., 1977. A theoretical study of receptor mechanisms in bacterial chemotaxis. SIAM J. Appl. Math. 32, 653–665.
Simpson, S.J., McCaffery, A.R., Hägele, B.F., 1999. A behavioural analysis of phase change in the desert locust. Biol. Rev. 74, 461–480.
Topaz, C.M., Bertozzi, A.L., 2004. Swarming patterns in a two-dimensional kinematic model for biological groups. SIAM J. Appl. Math. 65, 152–174.
Topaz, C.M., Bertozzi, A.L., Lewis, M.A., 2006. A nonlocal continuum model for biological aggregation. Bull. Math. Biol. 68, 1601–1623.
Uvarov, B., 1966. Grasshoppers and Locusts. Centre for Overseas Pest Research, London.
Vabø, R., Nøttestad, L., 1997. An individual based model of fish school reactions: Predicting antipredator behaviour as observed in nature. Fish. Oceanogr. 6, 155–171.
Vicsek, T., Czirok, A., Farkas, I.J., Helbing, D., 1999. Application of statistical mechanics to collective motion in biology. Physica A 274, 182–189.
Warburton, K., Lazarus, J., 1991. Tendency-distance models of social cohesion in animal groups. J. Theor. Biol. 150, 473–488.